Mechanically Induced Second Harmonic Generation in S_{C^*} Elastomers

Ingo Benné, Klaus Semmler, and Heino Finkelmann*

Institut für Makromolekulare Chemie, Universität Freiburg, Stefan-Meier-Strasse 31, D-79104 Freiburg, Germany

Received August 2, 1994; Revised Manuscript Received October 28, 1994®

ABSTRACT: A liquid crystalline elastomer (LCE) exhibiting a chiral smectic C phase (S_{C^*} phase) was synthesized and macroscopically ordered by mechanical deformations. The elastomer displays a permanent noncentrosymmetric structure and is therefore suitable for second harmonic generation (SHG) without applying external electrical poling fields. Using the Maker fringe experiment, the three largest nonlinear optical coefficients d_{ij} were measured and the temperature dependence observed. This liquid-crystal system represents a new class of material for nonlinear optics.

Introduction

The chiral smectic C phase (S_{C^*} phase) possesses smectic layers which exhibit a spontaneous polarization.[1] Due to the helicoidal superstructure of the S_{C^*} phase, however, no ferroelectricity but helielectricity occurs. Only an unwinding of this helicoidal structure yields samples with a macroscopic spontaneous polarization exhibiting point symmetry C_2. The C_2 symmetry implies that the untwisted S_{C^*} phase can exhibit second-order nonlinear optical (NLO) properties such as the linear electro-optic effect and second harmonic generation (SHG). Furthermore, the correct phase symmetry exists for phase-matched SHG to be observed.

To obtain the untwisted S_{C^*} phase structure different approaches exist. For low mass liquid crystals and linear liquid crystal polymers, the common practice is to apply an external electrical field or to use surface forces.[2–4] These methods, however, are limited to thin layers of the S_{C^*} material, with the additional difficulty for electrically poled systems being a possible reorientation process after removing the field. In contrast to this, liquid crystalline elastomers (LCE) can be macroscopically, uniformly oriented by mechanical deformations,[5] and this orientation process is not limited to thin samples or suitable dielectric anisotropy of the material. Furthermore, for LCEs the oriented structure can be chemically locked in by cross-linking, resulting in the so-called liquid single crystal elastomers (LSCE).[6]

In previous papers,[7,8] we have illustrated that an appropriate mechanical deformation of a S_{C^*} elastomer yields a permanent macroscopically, uniform orientation. This process also unwinds the helicoidal superstructure, and accordingly frequency doubling is observed where the intensity of the SHG is directly related to the perfection of the uniform smectic layer orientation.

In this paper, we present the quantitative analysis of Maker fringe experiments on these LCEs with respect to the absolute values of the nonlinear susceptibilities d_{ij}. The phase structure, the absolute values of the refractive indices, and the temperature dependence of the SHG signal will also be reported.

Synthesis and Preparation of the Elastomer

The LC elastomer was synthesized as described previously.[9] The elastomer contains two different mesogenic moieties statistically linked to a polysiloxane backbone (Figure 1). Although both mesogenic side groups provide a broad S_{C^*} phase, the chiral benzoic acid phenyl ester was used to shift the LC to isotropic transition to lower temperatures. The chiral benzoic acid biphenyl ester was laterally substituted with a nitro group to improve the NLO response.[10,11] The synthesis of this chromophore has recently been described by Kapitza et al.[12] Elastomer films of 300–500 μm thickness were prepared by the spin-casting technique in solution. Directly

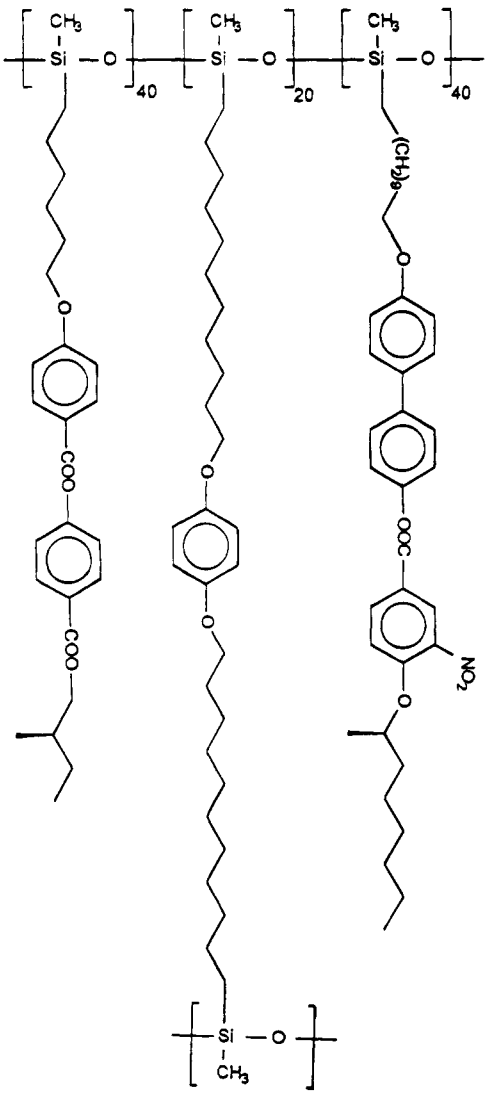

Figure 1. System under investigation.

® Abstract published in *Advance ACS Abstracts,* January 1, 1995.

0024-9297/95/2228-1854$09.00/0

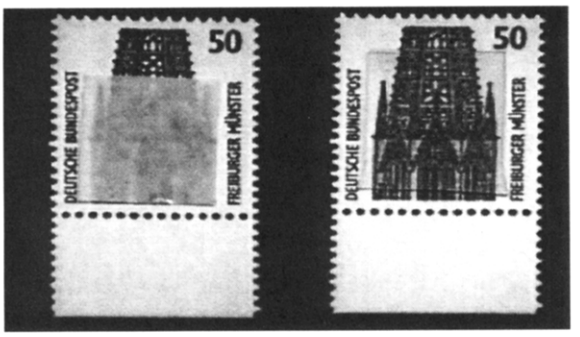

Figure 2. Photograph of the oriented S_{C^*} elastomer corresponding to the unoriented polydomain sample.

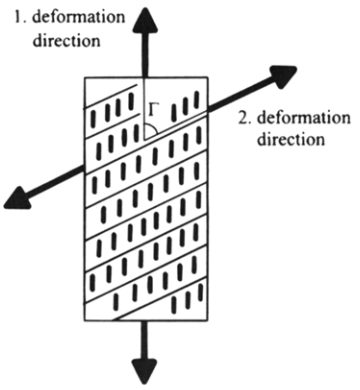

Figure 3. Structure of the chiral smectic C elastomer after the second deformation step.

after this process, before cross-linking is completed, the elastomer was mechanically ordered as described previously:[7,8] A swollen elastomer film was fixed at one end with a clamp, and the free-standing film is dried for 24 h at room temperature. During this drying process, the elastomer becomes liquid crystalline. Simultaneously, the elastomer becomes stretched with a stress of about 3×10^{-2} N mm^{-2}. This uniaxial deformation leads to a uniform orientation of the preferred direction (director) of the mesogen long axis parallel to the stress direction, and the smectic layers were ordered with an angle Φ of the layer normal to the mesogen long axis, where Φ is identical to the tilt angle of the mesogenic units in the smectic layer (chevron texture). Under these conditions, the cross-linking reaction proceeds and the mechanically induced anisotropic network structure and subsequent uniform director orientation are chemically locked-in. The samples are completely translucent, indicating "high order" in contrast to nonordered turbid samples (Figure 2). However, because of the conic layer structure the elastomer does not exhibit macroscopical C_2 symmetry and no SHG should be observed. To obtain a uniform layer orientation, a second uniaxial stress was applied under the angle $\Gamma = 90° - \Phi$ to the first deformation direction (refer to Figure 3). After removing the stress, the sample still exhibits the macroscopical, uniform orientation, owing to the cross-linking process. Therefore, the elastomer displays now permanently the correct symmetry and is suitable for SHG experiments.

Characterization of the Elastomer

The transition temperatures were analyzed by differential scanning calorimetry (DSC-7, Perkin-Elmer) and temperature-dependent X-ray measurements. Above the glass transition, at −7 °C, the elastomer exhibits a broad S_{C^*} phase up to 52 °C, followed by a S_A phase with a clearing temperature of 75 °C.

To quantify the macroscopic orientation of the sample, the elastomer was analyzed by X-ray measurements using a monochromatic Cu Kα (λ = 1.54 Å) beam. A two-dimensional image plate system (700 × 700 pixels, 250 μm/125 μm resolution) was used as the detector. The X-ray pattern of the film as obtained after the first deformation is shown in Figure 4a. As expected, the azimuthal wide-angle reflections representing the mesogen−mesogen distance display clear horizontal maxima indicating a uniform alignment of the mesogen long axes. The azimuthal small-angle reflections exhibit four maxima. The same pattern was obtained if the sample was rotated around the director of the mesogen long axis, indicating the conic layer orientation described above. The angle of the layer normal to the director has the value $\Phi = 22°$.

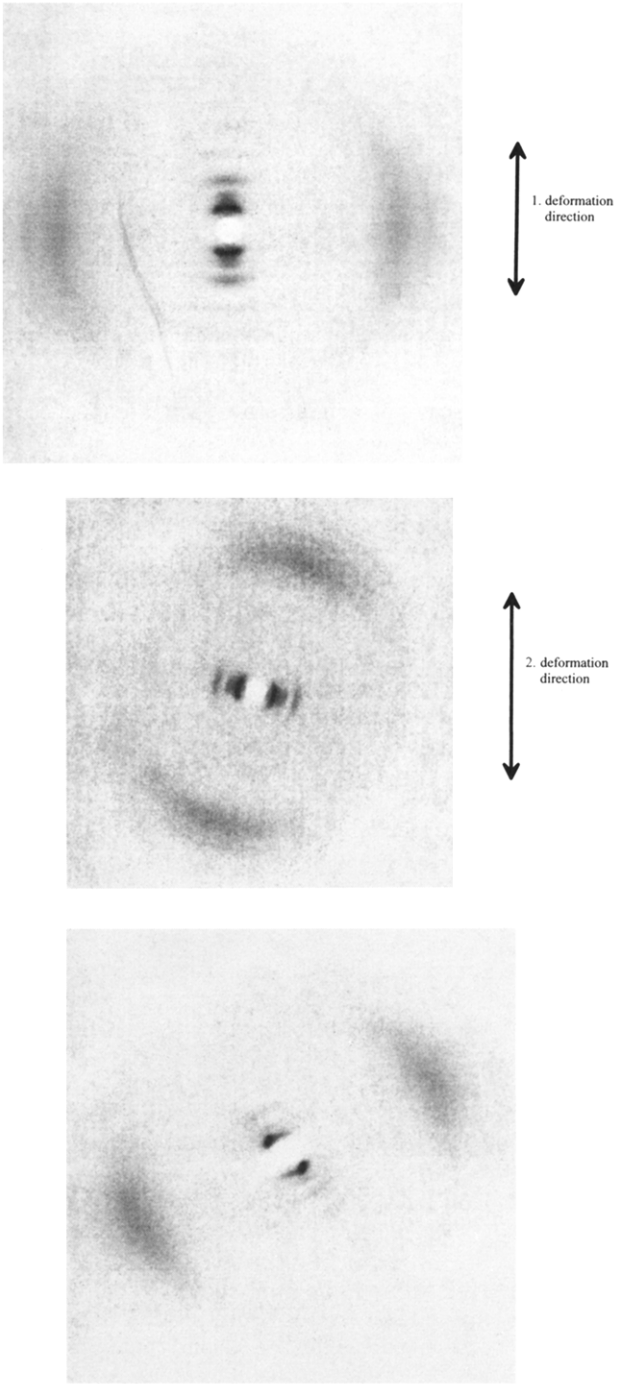

Figure 4. X-ray patterns of the S_{C^*} elastomer after uniaxial deformation (top (a)), of the nonannealed sample after the second deformation (middle (b)), and of the annealed sample (bottom (c)).

The X-ray pattern of the elastomer as obtained after the second deformation (alignment of the layer structure) is shown in Figure 4b. (Owing to a rotation of the

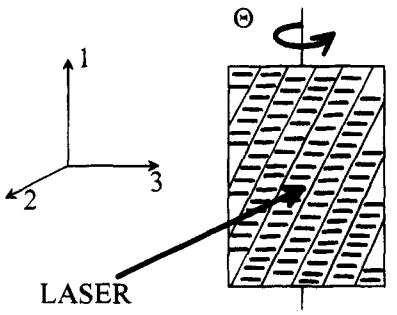

Figure 5. Experimental arrangement for the Maker fringe experiment together with the coordinate system.

sample, the X-ray pattern is rotated with respect to the X-ray pattern in Figure 4a.) Whereas no changes in the wide-angle reflections can be observed, the small-angle reflections now exhibit an asymmetric distribution of the intensities, indicating a nonsymmetric layer distribution. Obviously, under the present preparation conditions the layer orientation is not completed. We therefore annealed the elastomer within the S_{C^*} phase (50 °C) for 24 h. This procedure causes an excellent orientation of the layer structure and additionally induces a better orientation of the mesogen long axis as indicated by the two sharp maxima in the small-angle reflection and by the curtailment of the wide-angle reflection shown in Figure 4c.

The absolute values of the refractive indices at λ = 1064 nm (fundamental wave) and λ = 532 nm (second harmonic wave) were determined by measuring the angle of total reflection. For T = 21.5 °C for the nonannealed sample they are

$$n_o(2\omega) = 1.518 \pm 0.001 \qquad n_o(\omega) = 1.497 \pm 0.005$$

$$n_e(2\omega) = 1.622 \pm 0.001 \qquad n_e(\omega) = 1.584 \pm 0.005$$

and for the annealed sample

$$n_o(2\omega) = 1.516 \pm 0.001 \qquad n_o(\omega) = 1.495 \pm 0.005$$

$$n_e(2\omega) = 1.627 \pm 0.001 \qquad n_e(\omega) = 1.590 \pm 0.005$$

where $n_o(\omega)$ and $n_e(\omega)$ are the ordinary and the extraordinary refractive indices for the fundamental wave and $n_o(2\omega)$ and $n_e(2\omega)$ are the ordinary and the extraordinary refractive indices for the second harmonic wave, respectively.

Second Harmonic Generation

The NLO susceptibilities of the free-standing film were measured using a Maker fringe experiment. A Nd:YAG Laser (DCR 3G, Spectra Physics, λ = 1064 nm, pulse width 8 ns, 10 pulses/s) with a Gaussian beam profile was used as the fundamental light source. The sample was mounted on a temperature-controlled rotation stage, and the incident polarized fundamental light was focused onto the sample. After passing the sample, the fundamental wave was blocked by a cutoff filter (Schott, BG39) and a monochromator. The intensity of the SH beam was then detected by a photomultiplier (Hamamatsu, R928) connected to a boxcar averager (SRS, SR250). For absolute measurements of the d_{ij} coefficients, the SH signal was calibrated using a quartz crystal (010 orientation, d_{11} = 0.5 pm/V).

The sample geometry for the SHG experiment is outlined in Figure 5. The 3-axis denotes the director of the molecular long axis of the mesogenic moieties. For the annealed, highly ordered sample the intensity of the second harmonic beam was detected as a function of the angle Θ that describes the rotation of the sample around the 1-axis. Typical Maker fringes are shown in Figure 6, where the symbols indicate the measured data and the continuous line indicates the calculated fit. Both the fundamental and the resulting SH beams were p-polarized. A similar result was obtained for the nonannealed sample as shown in Figure 7. However, as we know from the X-ray pattern, this sample exhibits a weak smectic layer orientation and the SH intensities are therefore strongly decreased. As expected, no SH intensity was observed for the uniaxial deformed sample.

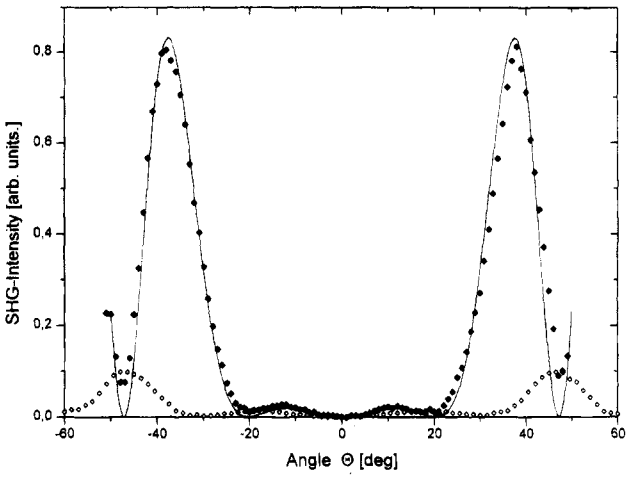

Figure 6. Maker fringe diagram for the annealed sample (◆) (including the data for the nonannealed sample (◇)). Θ indicates the rotation of the sample around the 1-axis (refer to Figure 5). The continuous line denotes the calculated fit.

Discussion

For the point group C_2, the second-order polarizations P_1, P_2, and P_3 along the axes 1, 2, and 3 shown in Figure 5 are given by

$$P_1 = 2d_{14}E_2E_3 + 2d_{16}E_1E_2$$

$$P_2 = d_{21}E_1^2 + d_{22}E_2^2 + d_{23}E_3^2 + 2d_{25}E_1E_3 \quad (1)$$

$$P_3 = 2d_{34}E_2E_3 + 2d_{36}E_1E_2$$

where d_{ij} are the elements of the second-order nonlinear susceptibility tensor and E_i are the electric field components of the fundamental wave. Assuming Kleinman symmetry, the number of independent coefficients is reduced to four with $d_{14} = d_{25} = d_{36}$, $d_{23} = d_{34}$, and $d_{16} = d_{21}$.

In our experiment for p-polarized fundamental light with $\mathbf{E} = E(0,\sin\Theta_\omega,\cos\Theta_\omega)$, where Θ_ω is the internal angle between the k vector of the incident fundamental wave and the layer normal of the sample front, the nonlinear polarization is given by

$$P_1 = 2d_{14}E^2 \sin\Theta_\omega \cos\Theta_\omega$$

$$P_2 = d_{22}E^2 \sin^2\Theta_\omega + d_{23}E^2 \cos^2\Theta_\omega \quad (2)$$

$$P_3 = 2d_{34}E^2 \sin\Theta_\omega \cos\Theta_\omega$$

For p-polarized fundamental light therefore, a p-polarized wave resulting from the nonlinear polarization P_2

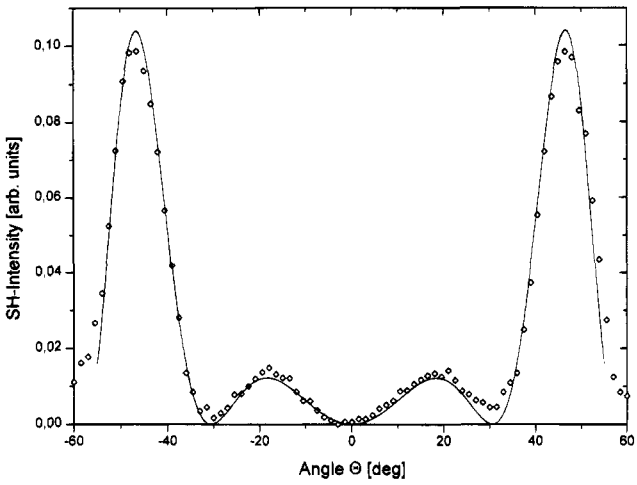

Figure 7. Maker fringe diagram for the nonannealed sample after the second mechanical deformation. Θ indicates the rotation of the sample around the 1-axis (refer to Figure 5). The continuous line denotes the calculated fit.

and P_3 as well as an s-polarized SH wave resulting from P_1 is expected. We have only analyzed the p-polarized SH wave resulting from a p-polarized fundamental wave since for the other polarizations the intensities were too small for a proper quantitative analysis.

Although the S_{C^*} phase is optically biaxial for the quantitative analysis of the Maker fringe experiments, we assume optical uniaxiality where the optical axis is parallel to the director of the mesogen long axes. For most known S_{C^*} systems two of the three refractive indices are identical within experimental error and the biaxiality can be neglected.[13,14]

The Maker fringe curves are described by the following theoretical expression[15]

$$I_{2\omega}(\Theta_\omega) \propto d_{eff}^2 t^4(\Theta_\omega)\, T(\Theta_\omega) \frac{1}{(n_\omega^2 - n_{2\omega}^2)^2} \sin^2 \Psi\, I_\omega^2 \tag{3}$$

where

$$\Psi = (\pi L/2)(4/\lambda)(n_\omega \cos \Theta_\omega - n_{2\omega} \cos \Theta_{2\omega}) \tag{4}$$

and

$$n_\omega = \left(\frac{\sin^2 \Theta_\omega}{n_o^2(\omega)} + \frac{\cos^2 \Theta_\omega}{n_e^2(\omega)}\right)^{-0.5}$$

$$n_{2\omega} = \left(\frac{\sin^2 \Theta_{2\omega}}{n_o^2(2\omega)} + \frac{\cos^2 \Theta_{2\omega}}{n_e^2(2\omega)}\right)^{-0.5} \tag{5}$$

Θ_ω and $\Theta_{2\omega}$ denote the internal angle of incidence for the fundamental and the second harmonic wave, respectively, I_ω is the intensity of the fundamental, and $I_{2\omega}$ is the intensity of the second harmonic wave. L is the sample thickness, λ is the wavelength of the fundamental, and $t(\Theta_\omega)$ and $T(\Theta_\omega)$ are transmission factors resulting from the boundary conditions.

For p-polarized fundamental light, the effective nonlinear susceptibility d_{eff} is given by

$$d_{eff} = d_{22} \sin^2 \Theta_\omega \sin \Theta_{2\omega} + d_{23}(\cos^2 \Theta_\omega \sin \Theta_{2\omega} + 2 \sin \Theta_\omega \cos \Theta_\omega \cos \Theta_{2\omega}) \tag{6}$$

To determine the d_{ij} coefficients the Maker fringe curves were theoretically fitted by eq 3. The fit is indicated in Figures 6 and 7 by the continuous line. For the annealed, highly ordered sample, we obtain values of

$$d_{22} = 0.10 \pm 0.05 \text{ pm/V}$$

$$d_{23} = d_{34} = 0.15 \pm 0.05 \text{ pm/V}$$

Although only 50% of the mesogenic units in our system contain the NLO-enhancing nitro group, these values are in the same order as the value of quartz ($d_{11} = 0.5$ pm/V) or as those for nitro-substituted biphenyl chromophores in low molecular weight LC systems.[14]

As expected, for the nonannealed sample we obtain much lower values.

$$d_{22} = 0.012 \pm 0.005 \text{ pm/V}$$

$$d_{23} = d_{34} = 0.05 \pm 0.01 \text{ pm/V}$$

In the temperature-dependent measurements many effects have to be accounted for. With the variation of the temperature, the sample thickness and the refractive indices change. For the S_{C^*} phase, the tilt angle of

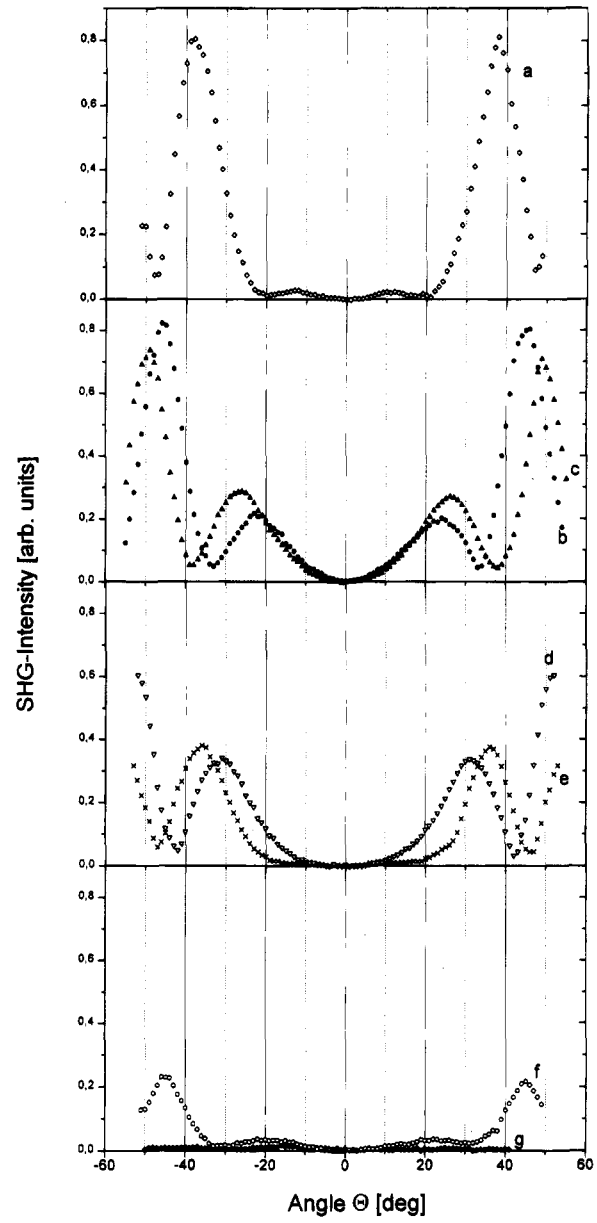

Figure 8. Temperature-dependent Maker fringe experiment for the annealed S_{C^*} elastomer: (a) 21.5, (b) 30.0, (c) 35.0, (d) 40, (e) 45, (f) 50, and (g) 55 °C.

the mesogens and therefore the optical axis shift and furthermore with increasing temperature the state of order of the liquid crystalline phase decreases. Due to both this decrease and the shift of the tilt angle to zero, it can be expected that the nonlinear susceptibilities decrease with increasing temperature and should vanish in the S_A phase.

In our measurement, a shift of the fringes can be observed (refer to Figure 8), which is related to the shift of the refractive indices and the sample thickness with temperature. As mentioned above, at higher temperatures the signal decreases and subsequently vanishes totally in the S_A phase at $T > 52$ °C. However, for the small-angle range ($-30° \leq \Theta \leq 30°$) it seems that the intensity of the fringes first increases with increasing temperature. This behavior can be explained with the angle dependence of the effective nonlinear susceptibility d_{eff}. For the small-angle range, the d_{eff} values enlarge strongly with increasing angle. Since the fringes shift to larger angles, the SHG intensities increase first although the absolute values of the d_{ij} coefficients decrease. As expected, in the S_A phase the sample does not exhibit the correct phase symmetry and the signal vanishes. After cooling into the S_{C^*} phase, the signal can be detected again.

For a quantitative analysis of the temperature-dependent measurements, the sample thickness as well as the refractive indices must be determined with varying temperature. Since the experimental error for these determinations is too large for a proper quantitative analysis, we chose not to determine the d_{ij} coefficients.

The C_2 symmetry of the untwisted S_{C^*} phase enables phase-matchable SHG to be observed. For homeotropically aligned low molar mass liquid crystals this has already been proved in several papers.[14,16] As our system exhibits a homogeneous alignment, the phase-matching angle is too large for a suitable light coupling. However, for thicker elastomers it should be possible to couple the light into the edge of the sample at an appropriate angle for phase matching.

Conclusion

Our measurements, for the first time, reveal that it is possible to transform S_{C^*} elastomers into permanently oriented samples by suitable mechanical deformations. Thus samples exhibiting macroscopical C_2 symmetry are obtained without any external electric poling fields. The observed nonlinear susceptibilities are in the same order as those for similar chromophores in low molecular weight systems. It has to be noted that only 50% of the mesogenic units in our system are (not optimized) chromophores. Using more suitable chromophores much larger susceptibilities should be observed as already exemplified for low molar mass S_{C^*} systems.[16] With respect to this it is conceivable to synthesize elastomers with our method that equal most organic and inorganic single crystals or conventional polymeric systems. The processing and handling of the LC elastomer, however, are more practicable and not limited to crystal growth. This liquid crystal system therefore represents a new class of material for nonlinear optical applications.

References and Notes

(1) Meyer, R. B.; Liébert, L.; Strzelecki, L.; Keller, P. *J. Phys. (Paris), Lett.* **1975**, *36*, L69.
(2) Shtykov, N. M.; Barnik, M. I.; Beresnev, L. A.; Blinov, L. M. *Mol. Cryst. Liq. Cryst.* **1985**, *124*, 379.
(3) Poths, H.; Schönfeld, A.; Zentel, R.; Kremer, F.; Siemensmeyer, K. *Adv. Mater.* **1992**, *4*, 351.
(4) Clark, N. A.; Lagerwall, S. T. *Appl. Phys. Lett.* **1980**, *36*, 899.
(5) McArdle, C. B., Ed. *Side-Chain Liquid Crystalline Polymers*; Blackie and Son: Glasgow, U.K., 1989.
(6) Küpfer, J.; Finkelmann, H. *Makromol. Chem., Rapid Commun.* **1991**, *12*, 717.
(7) Semmler, K.; Finkelmann, H. *Polym. Adv. Tech.* **1994**, *5*, 231.
(8) Benné, I.; Semmler, K.; Finkelmann, H. *Macromol. Rapid Commun.* **1994**, *15*, 295.
(9) Finkelmann, H.; Kock, H. J.; Rehage, G. *Makromol. Chem., Rapid Commun.* **1981**, *2*, 317.
(10) Walba, D. M.; Ros, M. B.; Clark, N. A.; Shao, R.; Johnson, K. M.; Robinson, M. G.; Liu, J. Y.; Doroski, D. Design of Ferroelectric Liquid Crystals for Electronic NLO Applications. In *Materials for Nonlinear Optics: Chemical Perspectives*; Marder, S. R., Stucky, G. D., Sohn, J. E., Eds.; ACS Symposium Series 455; American Chemical Society: Washington, DC, 1991.
(11) Walba, D. M.; Ros, M. B.; Clark, N. A.; Shao, R.; Johnson, K. M.; Robinson, M. G.; Liu, J. Y.; Doroski, D. *Mol. Cryst. Liq. Cryst.* **1991**, *198*, 51.
(12) Kapitza, H.; Zentel, R.; Twieg, R. J.; Nguyen, C.; Vallerien, S. U.; Kremer, F.; Willson, C. G. *Adv. Mater.* **1990**, *11*, 539.
(13) Liu, J. Y.; Robinson, M. G.; Johnson, K. M.; Walba, D. M.; Ros, M. B.; Clark, N. A.; Shao, R.; Doroski, D. *J. Appl. Phys.* **1991**, *70*, 3426.
(14) Yoshino, K.; Utsumi, M.; Morita, Y.; Sadohara, Y.; Ozaki, M. *Liq. Cryst.* **1993**, *14*, 1021.
(15) Jerphagon, J.; Kurtz, S. K. *J. Appl. Phys.* **1970**, *41*, 1667.
(16) Schmitt, K.; Herr, R.-P.; Schadt, M.; Fünfschilling, J.; Buchecker, R.; Chen, X. H.; Benecke, C. *Liq. Cryst.* **1993**, *14*, 1735.

MA941105N